ISSN 0030-400X, Optics and Spectroscopy, 2013, Vol. 115, No. 5, pp. 660–665. © Pleiades Publishing, Ltd., 2013.
Original Russian Text © N.V. Rudakova, I.V. Timofeev, S.Ya. Vetrov, 2013, published in Optika i Spektroskopiya, 2013, Vol. 115, No. 5, pp. 747–752.

CONDENSED-MATTER SPECTROSCOPY

Optical Properties of Nanostructured 2D Metal–Dielectric Photonic Crystals with a Lattice Defect

N. V. Rudakova[a], I. V. Timofeev[b], and S. Ya. Vetrov[a]

[a] *Siberian Federal University, Krasnoyarsk, 660074 Russia*

[b] *Kirensky Institute of Physics, Russian Academy of Sciences, Siberian Branch, Krasnoyarsk, 660036 Russia*

e-mail: atrum528@mail.ru; tiv@iph.krasn.ru

Received January 25, 2013; in final form, March 4, 2013

Abstract—Optical properties of 2D nanocomposite-based photonic crystals with a lattice defect are studied. The nanocomposite comprises metallic nanospheres dispersed in a transparent matrix and is characterized by an effective resonant permittivity. Transmission spectrum for *s*-polarized waves at oblique incidence is calculated. Spectral manifestation of the splitting of the defect mode when its frequency coincides with the resonant frequency of the nanocomposite is studied. The essential dependence of the splitting on the angle of incidence and concentration of metallic nanospheres in the nanocomposite matrix is established. Specific features of spatial distribution of the electric field intensity in defect modes of crystals are analyzed.

DOI: 10.1134/S0030400X13110209

INTRODUCTION

Photonic crystals (PCs), the dielectric properties of which vary periodically with a period admitting Bragg diffraction of light, are attracting considerable interest as new optical materials with unique properties [1–3]. One important property of a PC is related to the localization of electromagnetic waves on defects of the structure [4–7]. In this case, additional allowed levels corresponding to localized defect modes arise in the bandgap (BG) of the PC. The position and transmission coefficient of defect modes can be efficiently controlled by varying the geometrical and structural parameters of the PC. PCs with defect modes have been used to create new types of photonic-crystal fibers [8] and high-Q nanocavities and low-threshold lasers [9], as well as to propose ways to increase the efficiency of nonlinear-optical processes [10, 11]. Composite media with metal nanoparticles for manufacturing nanostructured metal–dielectric PCs and creating, on their basis, new methods of light control are of great interest [12]. It has been predicted that, in a nanocomposite comprised of metal nanoparticles suspended in a transparent matrix, there should arise a resonance of the effective permittivity [13, 14] (with no resonant features in optical characteristics of the original materials). The position of the resonance, lying in the optical range, depends on the permittivity of the original materials, as well as on the concentration and shape of nanoparticles.

In this paper, using the modified transfer-matrix method [15], we study the spectral properties and spatial distribution of the electric-field intensity in defect modes of 2D photonic crystals prepared from a nanocomposite. The nanocomposite consists of metallic nanoparticles dispersed in a transparent matrix and is characterized by effective resonant permittivity $\varepsilon_{\text{mix}}(\omega)$.

DESCRIPTION OF MODEL

Consider, as in [15, 16], resonant photonic crystals (RPCs) of two types. The crystals are assumed to be shaped as plates boundless in two directions, to have a finite thickness, and to be in vacuum. The RPC of type (a) consists of infinite cylindrical holes forming a square lattice in the nanoocomposite matrix. The linear defect is created by filling the middle row of the holes with the nanocomposite (Fig. 1a). The structural elements of the type (b) crystal are nanocomposite cylinders forming a square lattice in the air ($\varepsilon = 1$). The linear defect is created by removing the middle row of the cylinders (Fig. 1b). The nanocomposite consists of spherical nanoparticles of silver randomly distributed over the transparent dielectric matrix. We assume that the axes of the cylinders are perpendicular to the xy plane and parallel to the z axis, while centers of cross sections of the cylinders in the plane xy form a square lattice. The *s*-polarized waves propagate in the plane xy at the angle θ with respect to the x axis.

In calculations, we used, as in [15], the following parameters for silver: $\varepsilon_0 = 5$, $\omega_p = 9$ eV, and $\gamma = 0.02$ eV. For the matrix, we assumed $\varepsilon_d = 9$, period of the PC structure $d = 150$ nm, and plate thickness $L = 7d$; the composite filling factor was

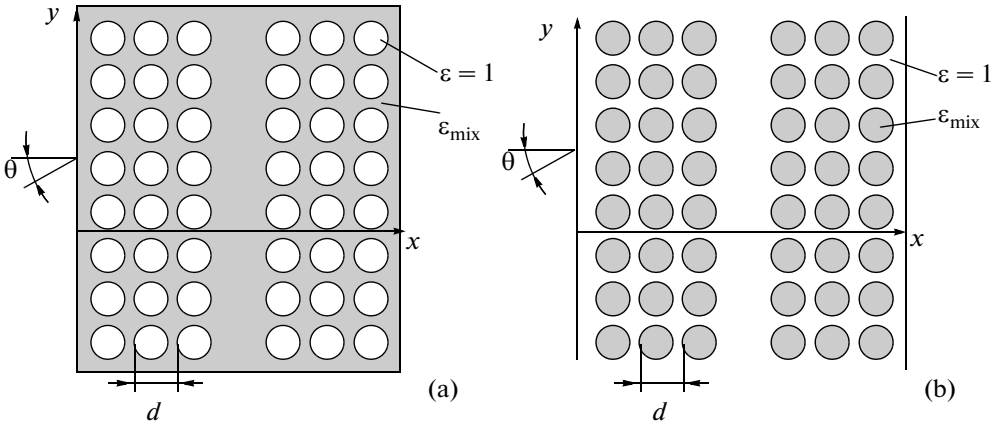

Fig. 1. Schematic diagram of the 2D PC structure with a defect layer comprised of seven rows: d is lattice period, θ is the angle of incidence, (a) cylindrical hole form a square lattice in the nanocomposite matrix, the defect is created by filling by the nanocomposite of middle row of cylindrical holes, (b) nanocomposite cylinders form a square lattice in the air (ε = 1), the defect is created by removing the middle row of the cylinders.

determined by the expression $F = \pi r^2/d^2 = 0.5$, where r is the cylinder radius.

Permittivity ε_{mix} is given by the Maxwell–Garnett equation, which is commonly used for the description of matrix media when the host matrix contains isolated inclusions of small volume fraction [13, 17, 18],

$$\varepsilon_{mix} = \varepsilon_d\left[1+\frac{f}{(1-f)/3+\varepsilon_d/(\varepsilon_m-\varepsilon_d)}\right], \qquad (1)$$

where f is the filling factor, i.e., the fraction of nanoparticles in the matrix; $\varepsilon_m(\omega)$ and ε_d are the permittivities of the nanoparticle metal and matrix, respectively; and ω is the optical frequency. The size of a nanoparticle is much smaller than the light wavelength and depth of the field penetration into the material. The permittivity of the metal of nanoparticles can be found using the Drude approximation

$$\varepsilon_m(\omega) = \varepsilon_0 - \omega_p^2/\omega(\omega + i\gamma), \qquad (2)$$

where ε_0 is a constant that takes into account contributions of the interband transitions of bound electrons, ω_p is the plasma frequency, and γ is the inverse relaxation time of electrons.

The function $\varepsilon_{mix}(\omega)$ is complex:

$$\varepsilon_{mix}(\omega) = \varepsilon'_{mix}(\omega) + i\varepsilon''_{mix}(\omega).$$

Neglecting small factor γ^2, we can find the plasmon resonance frequency, which depends on characteristics of the initial materials and concentration of dispersed phase f:

$$\omega_0 = \omega_p\sqrt{(1-f)/[3\varepsilon_d + (1-f)(\varepsilon_0 - \varepsilon_d)]}. \qquad (3)$$

At the point $\omega = \omega_0$, the function $\varepsilon'_{mix}(\omega)$ turns into zero, while $\varepsilon''_{mix}(\omega)$ acquires the greatest value. The function $\varepsilon'_{mix}(\omega)$ also turns into zero at the point

$$\omega_1 = \omega_p\sqrt{(1+2f)/[\varepsilon_0 + 2\varepsilon_d + 2f(\varepsilon_0 - \varepsilon_d)]}. \qquad (4)$$

At the interval $[\omega_0, \omega_1]$, the function $\varepsilon'_{mix}(\omega) < 0$, i.e., the nanocomposite, in this frequency region, is akin to metal.

The 2D photonic crystals with linear defects of both types (Fig. 1) were prepared using the technique of electron-beam lithography [19, 20]. The periodic array of cylindrical holes is usually etched in the semiconductor layer with a period lying in the interval 0.6–1.2 μm. Today, the most interesting PCs are with the BG lying in the visible (λ = 400–700 nm) or near-IR (λ = 1–1.5 μm) spectral range [21]. 2D photonic crystals based on nanochannel glass plates made it possible to implement the BG in the spectral range between 500 and 600 nm [22]. The nanocomposite matrix for the PCs under consideration can be prepared on the basis of optical glass with dispersed silver nanoparticles. At present, commercially manufactured optical glasses are transparent in the visible and IR ranges and are characterized by the refractive index variable in a wide range. A nanocomposite from glass and silver nanoparticles may be prepared using the technology described in [23].

RESULTS OF CALCULATIONS AND DISCUSSION

Consider, first, the results of calculations for a plate of the 2D RPC of type (a) (Fig. 1a). Figure 2 shows the transmission spectrum for the *s*-polarized waves incident on the PC plate normal to the linear defect of the

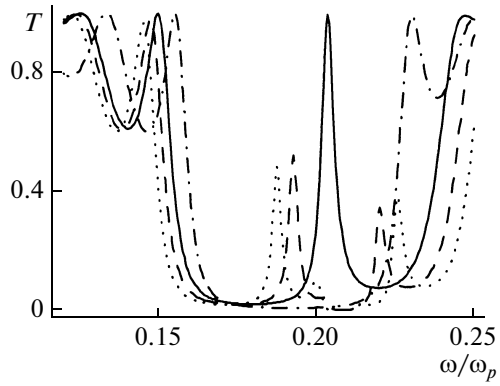

Fig. 2. The transmission coefficient as a function of frequency for the (a)-type crystal for the angle of incidence θ = 0: PC with no defect, $f = 0$ (dash-dotted line); PC with the defect, $f = 0$ (solid line). Splitting of the defect mode at $f = 0.005$ (dashed line) and $f = 0.01$ (dotted line).

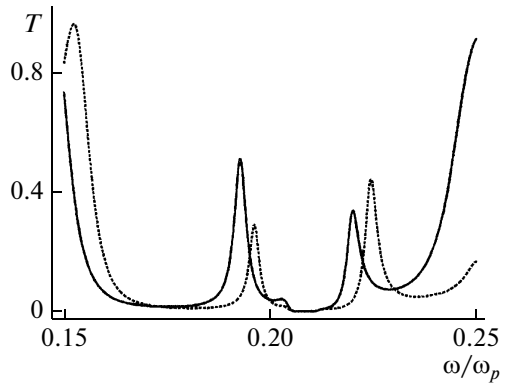

Fig. 3. Transmission spectrum for the (a)-type crystal at different values of the angle of incidence, $f = 0.005$: θ = 0° (solid line) and 45° (dashed line).

structure. As seen from the figure, the defect induces a transmission peak in the BG corresponding to the defect mode. When the defect mode frequency coincides with the resonance frequency of the nanocomposite ω_0, the defect mode exhibits splitting similar to that of two coupled oscillators, which increases with increasing concentration of silver nanospheres in the nanocomposite.

The calculations show that, with increasing factor of filling by silver particles from 0.005 to 0.02, i.e., fourfold, the splitting increases by a factor of 2 and reaches 54 nm. The BG width also continuously increases with increasing concentration of the nanospheres in the matrix.

Characteristic dependence of the transmission spectrum on angle of incidence θ is shown in Fig. 3. As θ changes, there arises a detuning between resonance frequency ω_0 and the defect-mode frequency. The intensity at the peak of the low-frequency mode noticeably decreases, while intensity of the high-frequency mode increases.

With increasing angle of incidence, the BG bounds shift toward higher frequencies in accordance with the Bragg condition. The frequencies of the two defect modes in the BG of the PC structure also shift toward higher frequencies. Such a behavior of these frequencies can be understood by considering the defect mode of the PC structure as a standing wave arising due to reflection from the walls of the cavity formed by the nanodefect with a thickness of W_d. If we, in addition, neglect the frequency dependence of the refractive index in the region of the transmission peaks, then the resonance condition acquires the form

$$\lambda = 2W_d\sqrt{n^2 - \sin^2\theta},$$

where n is the refractive index of the defect layer.

Therefore, as the angle of incidence increases, the mode frequencies shift toward high frequencies, which is observed in the numerical simulation.

Analysis of the spatial distribution of the electric-field intensity shows that, for both modes, the field is localized in the region of the defect comparable in size with the light wavelength. At defect-mode frequency ω_0, for $f = 0$, and at frequencies of the low-frequency and high-frequency peaks for $f = 0.005$ (see Fig. 2), the character of the field distribution inside the sample is practically the same (Fig. 4). The greatest intensities of the field at the defect-mode frequencies are reached in interstitial sites in the vicinity of the linear defect. However, the maximum intensity of localization of the high-frequency peak at $f = 0.005$ decreases by a factor of 3 (Fig. 4f) as compared with the maximum at the defect-mode frequency (Fig. 4b), while the maximum intensity of localization of the low-frequency peak decreases nearly by a factor of 2 (Fig. 4d).

Consider now the results obtained for the RPC sample of type (b) with a linear defect in the form of a removed row of nanocylinders (Fig. 1b). As was already mentioned [15], transmission spectra of the finite ideal RPCs of both types in the region of the BG practically do not differ provided that their composite filling factors F, along with other parameters, are the same. Figure 5a illustrates, as an example, such coincidence of the transmission spectra for the case in which, for both RPCs, $F = 0.5$, and the fraction of the nanospheres in the nanocomposite is $f = 0$. However, the transmission spectra of the crystals with defects of both types, for which $F = 0.5$ and $f = 0$ with all other parameters the same, are different (Fig. 5b). As is seen from the figure, the defect-mode frequencies are essentially different.

Such behavior of these frequencies can be understood by considering the defect mode of the PC structure as a standing wave arising due to reflection from identical multilayer mirrors or, in other words, from walls of the cavity formed by the nanodefect with

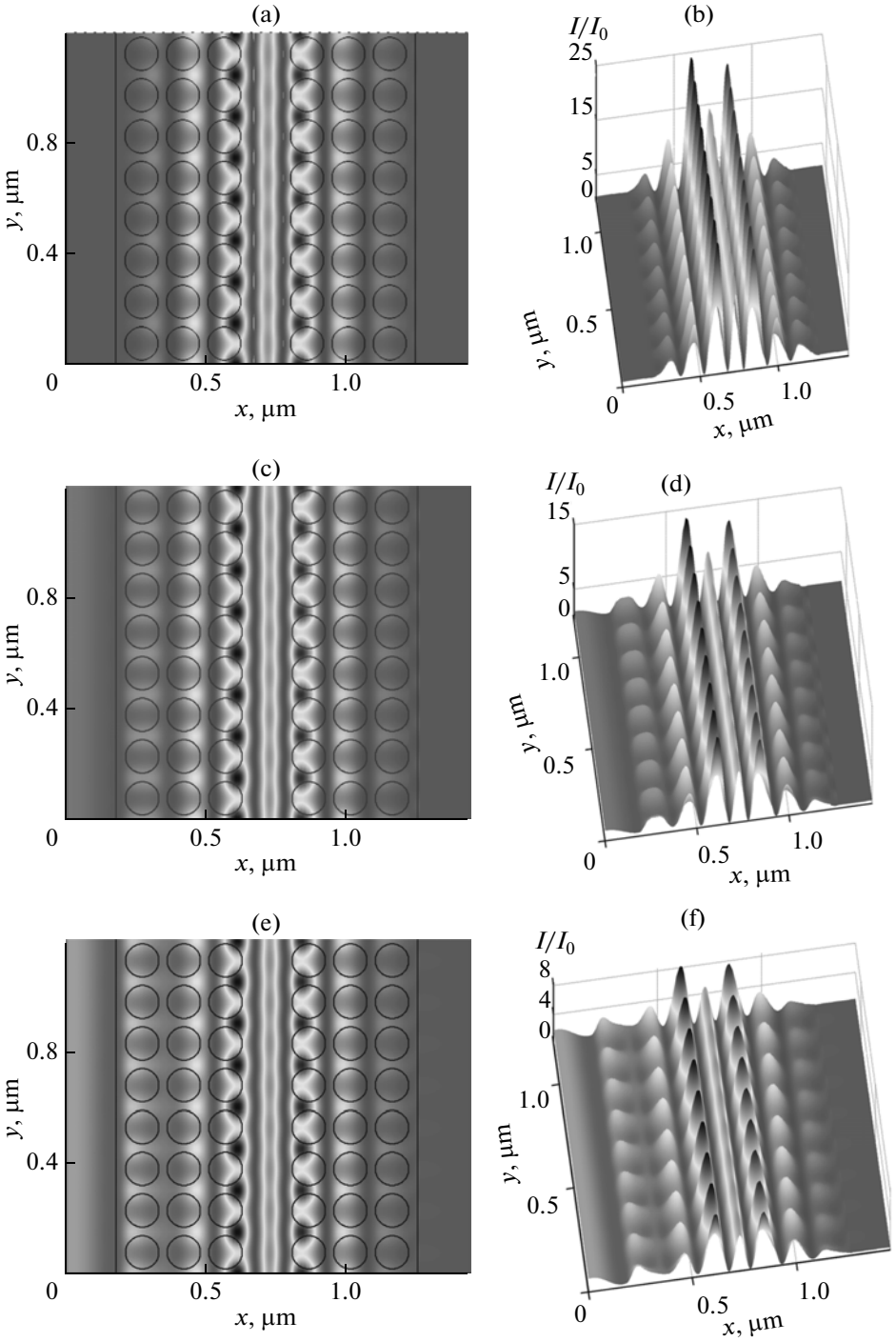

Fig. 4. Spatial-intensity distribution normalized to intensity I_0 of the incident light for the (a)-type crystal: at the frequency of the defect mode, $\theta = 0, f = 0$, (a) top view, (b) side view; at the frequency of low-frequency peak of the split defect mode, $\theta = 0, f = 0.005$, (c) top view, (d) side view; at the frequency of the high-frequency peak of the split-defect mode, $\theta = 0, f = 0.005$, (e) top view, and (f) side view.

width W_d. The condition of resonance at normal incidence of the light has the form $\lambda = 2W_d n$. Therefore, the frequency of the defect mode of the type (b) RPC should exceed the type (a) crystal frequency, which is confirmed by the numerical simulation. The calculations show that the behavior of the defect modes of the RPCs of both types with angle of incidence and concentration of the nanospheres in the nanocomposite is the same. It was also shown that, for the RPCs of both types, the field in the defect modes is localized in the

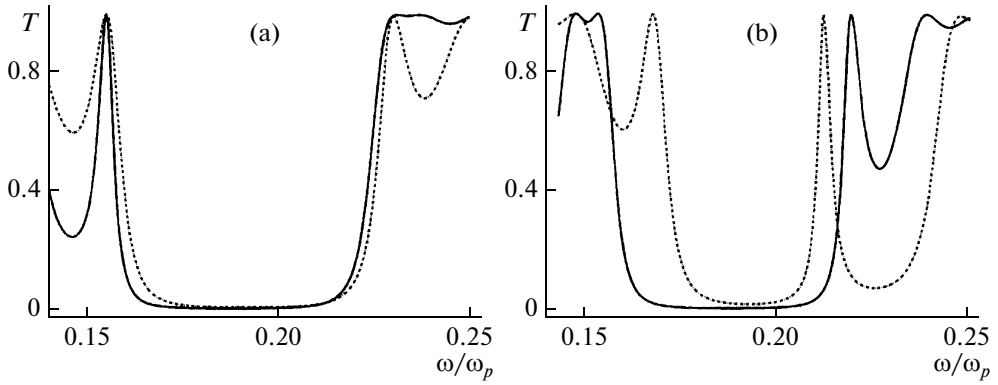

Fig. 5. Transmission spectra of the crystals with no defect (a) and crystals with linear defects (b). Dash-dotted line refers to (a)-type crystals, solid line pertains to (b)-type crystals. $F = 0.5, f = 0$.

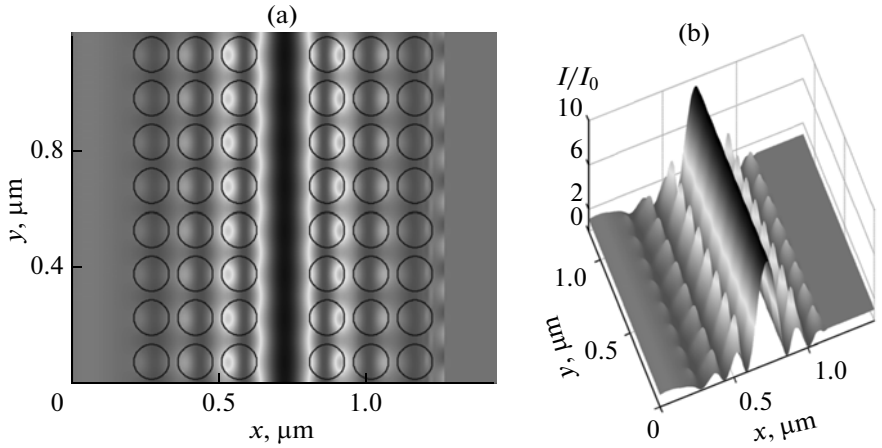

Fig. 6. Spatial-intensity distribution normalized to intensity I_0 of the incident light for the (b)-type crystal. At frequency of the defect mode $\theta = 0, f = 0$, (a) top view, (b) side view.

region of the defect comparable in size with the light wavelength. However, distributions of the electric-field intensity in the RPCs of different types show qualitative distinctions—namely, in the (a)-type crystals the field is localized in the nanocomposite matrix, reaching its greatest value on interstitials near the linear defect, while, in the (b)-type crystals, this occurs in the nanocomposite rods with the greatest value on the defect (Fig. 6). The greatest values of the field intensity in defect modes of the (a)-type RPC exceed the field intensity in the corresponding defect modes of the (b)-type RPC. For instance, by comparing Figs. 4b and 6b, one can see that, at normal incidence, with concentration of the nanospheres $f = 0$ and filling factor $F = 0.5$, the greatest field intensity in the defect mode of the (a)-type crystal is twice as high as in the defect mode of the (b)-type crystal.

CONCLUSIONS

We studied the optical properties of 2D resonant photonic crystals of two types. In one of them, the linear defect is created by filling by a nanocomposite the middle row of cylindrical holes forming a square lattice in a nanocomposite matrix. In the other, the defect is created by removing the middle row of the nanocomposite cylinders forming a square lattice in vacuum. The results are obtained using the modified transfer-matrix method. It is shown that splitting of the defect mode is fairly sensitive to the concentration of nanoparticles and may reach 50 nm. The light field in the defect nodes is localized in the region comparable with the light wavelength with the greatest values of the field intensity in interstitials either near the defect or on the defect for crystals of types (a) and (b), respectively. Note that the 2D resonant photonic crystals with structural defects based on the nanocomposite with dispersed nanospheres allow one to work in the visible range.

To obtain the needed spectral characteristics of the resonance PC, one may use the resonance of the defect layer filled by other metal nanospheres with other geometrical parameters of the PC structure.

ACKNOWLEDGMENTS

This work was supported by the grants g/k 14.V37.21.0730 of the federal targeted program "Scientific and Pedagogical Personnel of Innovative Russia"; no. 24.29 of Presidium of the Siberian Branch of the Russian Academy of Sciences; the Ministry of Education and Science of the Russian Federation, Agreement 14.V37.21.0730; OFN RAS no. III.9.5; Presidium of RAS nos. 24.29 and 24.31; and Siberian Branch of the Russian Academy of Sciences, nos. 43 and 101.

REFERENCES

1. R. D. Meade and J. N. Winn, *Photonic Crystals* (Princeton Univ. Press, Princeton, 1995).
2. K. Sakoda, *Optical Properties of Photonic Crystals* (Springer, Berlin, 2004).
3. K. Busch, S. Lölkes, R. B. Wehrspohn, et al., *Photonic Crystals: Advances in Design, Fabrication and Characterization* (Wiley-VCH, Weinheim, 2004).
4. S. John, Phys. Rev. Lett. **58**, 2486 (1987).
5. D. R. Smith, R. Dalichaouch, N. Kroll, et al., J. Opt. Soc. Am. **10**, 314 (1993).
6. A. M. Zheltikov, S. A. Magnitskii, and A. V. Tarasishin, Zh. Eksp. Teor. Fiz. **117** (4), 691 (2000).
7. S. Ya. Vetrov and A. V. Shabanov, Zh. Eksp. Teor. Fiz. **120**, 1126 (2001).
8. A. M. Zheltikov, Usp. Fiz. Nauk **170**, 1203 (2000).
9. O. Painter, R. K. Lee, A. Scherer, et al., Science **284**, 1819 (1999).
10. M. G. Martem'yanov, T. V. Dolgova, and A. A. Fedyanin, Zh. Eksp. Teor. Fiz. **125** (3), 527 (2004).
11. T. V. Dolgova, A. I. Maidykovskii, M. G. Martem'yanov, et al., Pis'ma Zh. Eksp. Teor. Fiz. **73** (1), 8 (2001).
12. S. G. Tikhodeev and N. A. Gippius, Usp. Fiz. Nauk **179** (9), 1003 (2009).
13. A. N. Oraevskii and I. E. Protsenko, Kvantovaya Elektron. **31** (3), 252 (2001).
14. A. Sihvola, *Electromagnetic Mixing Formulas and Applications* (Institution of Engineering and Technology, London, 2008).
15. S. Ya. Vetrov, I. V. Timofeev, and N. V. Rudakova, Opt. Spektrosk. **112** (4), 638 (2012).
16. S. Ya. Vetrov, I. V. Timofeev, and N. V. Rudakova, Fiz. Tverd. Tela **53** (1), 133 (2011).
17. J. C. Maxwell-Garnett, Philos. Trans. Roy. Soc. **203**, 385 (1904).
18. L. A. Golovan', V. Yu. Timoshenko, and P. K. Kashkarov, Usp. Fiz. Nauk **177** (6), 619 (2007).
19. E. Istrate and E. H. Sargent, Rev. Mod. Phys. **78**, 455 (2006).
20. M. Tokushima, M. H. Yamada, and Y. Arakava, Appl. Phys. Lett. **84**, 4298 (2004).
21. O. Toader and S. John, Science **292**, 1133 (2001).
22. H.-B. Lin, R. J. Tonucci, and A. J. Campillo, Opt. Lett. **43**, 94 (1998).
23. D. Wang, S. Guo, and S. Yin, Opt. Eng. **42**, 3585 (2003).

Translated by V. Zapasskii